Hindawi
International Journal of Antennas and Propagation
Volume 2022, Article ID 3458705, 8 pages
https://doi.org/10.1155/2022/3458705

Research Article

Instantaneous Bandwidth Enhancement for Variable Inclination Continuous Transverse Stub Antenna

Zheng Liu, Jian Zhang, Xue Lei, Tianpeng Li, Jun Gao, and Zhijian Xu

National Digital Switching System Engineering and Technological R&D Center, Zhengzhou, China

Correspondence should be addressed to Zheng Liu; lz1994cn@163.com

Received 29 December 2021; Revised 10 May 2022; Accepted 30 June 2022; Published 14 July 2022

Academic Editor: Chien-Jen Wang

In this paper, a method was developed to achieve the instantaneous bandwidth enhancement of a variable inclination continuous transverse stub (VICTS) antenna. The aperture of the VICTS antenna was divided into a subarray, and the true-time delay was introduced to reduce the dispersion of the antenna. The method has low loss and is suitable for the entire beam scanning range. To demonstrate this method, a proposed VICTS antenna composed of 2×2 subarrays was designed and simulated. Compared with the traditional VICTS antenna of the same aperture size, the gain loss was reduced by at least 52% and the 3/4-dB gain-loss bandwidth increased from 2.5% to 4.2%. The impedance bandwidth of 16.7% with the S_{11} value of each subarray below −15 dB was achieved, and the sidelobe of the whole antenna was below −10 dB. The antenna radius was 0.34 m, and the aperture efficiency was 14.8%. The proposed antenna is a suitable candidate as a gateway station antenna for low earth orbit (LEO) satellite communication.

1. Introduction

With the popularity of low earth orbit (LEO) satellite communication, very small aperture terminal (VSAT) satellite antennas have developed rapidly [1]. There are three typical kinds of VSAT antennas: parabolic antennas, flat-panel antennas, and phased array antennas. Although parabolic antennas have the advantages of high gains and wide instantaneous bandwidths, their profiles are large. Flat-panel antennas [2] have small profiles but suffer from broad beamwidths, which can easily cause interference between adjacent satellites. Phased array antennas can be classified as active and passive phased array antennas. Active phased array antennas suffer from high power consumption, high mutual-coupling [3], and difficult calibration. Although there are many other kinds of antennas, such as metasurface [4] and continuous transverse stub (CTS) antennas, these antennas cannot achieve full-space beam scanning with low profiles or continuous polarization control.

Passive phased array antennas, such as the variable inclination continuous transverse stub (VICTS) antenna, have the advantages of low profiles, large impedance bandwidths, high gains, and high cross-polarization isolation. Thus, they are suitable for satellite communication. However, the VICTS antenna has some disadvantages, including roll-off losses as the main beam moves off-axis at larger scan angles and during frequency scanning. Frequency scanning means that for a fixed target, the gain changes with the frequency. That is, the instantaneous bandwidth is low. The instantaneous bandwidth is significant for communication, as it impacts the signal-to-noise ratio. For a signal with a given frequency and bandwidth, a small instantaneous bandwidth will decrease the signal-to-noise ratio, which is adverse for communication.

Recently, VICTS antennas have been studied by many researchers [5–9]. Gao et al. [6] proposed a theoretical model for the nonlinear slow-wave structure of the VICTS antenna [6]. A dual-band shared-aperture VICTS antenna working at K- and Ka-bands were investigated [7], and a V-band VICTS antenna was studied [8]. However, the dispersive nature of these antennas was not changed. For satellite communication, the instantaneous bandwidth is important. The magnitude distortion caused by beam squint will degrade the performance of the communication system.

The instantaneous bandwidth of an antenna can be increased by three means as follows: (1) selecting a material with dispersive behaviours [9], (2) introducing a true time delay [10], and (3) using active devices [11]. The approaches using active devices and materials with dispersive behaviours suffer from high losses. Therefore, the true time delay may be the best choice for a VICTS antenna. True time delay can be achieved by using a true time delay device or the length difference of the waveguide between each subarray. An example of the VICTS antenna with true time delay was proposed [12], but the theoretical analyses and the design methods were not provided.

In this paper, we propose a theoretical analysis method for the instantaneous bandwidth enhancement of the VICTS antenna and present the design methodology for the antenna. This analysis proved that the phase difference between each subarray is constant under different rotation angles of the radiation layer, which is the theoretical basis through which the instantaneous bandwidth of the VICTS antenna can be enhanced using a fixed true time delay. Based on the theoretical analysis, we propose a design method for the antenna.

This paper is organized as follows: Section 2 describes the analysis of the antenna based on array theory, and a design method is proposed based on the analysis. Section 3 describes the simulation results for the proposed VICTS antenna composed of 2×2 subarrays. Full-wave simulations of the array were performed using the time-domain solver of the CST Microwave Studio software. The main conclusions of this theoretical study are summarized in Section 4.

2. Analysis and Array Design

The structure of the VICTS antenna is shown in Figure 1. The antenna comprises three kinds of layers: polarization control, radiation, and feeding layers. The polarization control layers change the polarization of the antenna, which can change the polarization angle of the linear polarized wave. The radiation layer is composed of transverse stubs, and the electromagnetic power is radiated from the slots between the stubs. The feeding layer is mainly composed of the feeding structure and a corrugated plane, which is also called the slow-wave structure. The radiation layer, together with the feeding layer, forms a parallel plate waveguide structure, and the rotation of the radiation layer changes the phase relation between the slots, which controls the beam pointing of the VICTS antenna. Therefore, only the radiation layer and the feeding layer will be discussed in this paper.

The pattern of the traditional VICTS antenna was studied by Porter [5]. The antenna can be considered an array, as shown in Figure 2(a), and an equivalent triangular grid array is used to obtain the phase relation between each element. The beam pointing angle can be found to be

$$u = \sin(\theta)\cos(\phi) = \frac{\lambda}{d} * \sin(\gamma), \tag{1a}$$

$$v = \sin(\theta)\sin(\phi) = -\frac{\lambda}{d} * \cos(\gamma) + \sqrt{\epsilon_g}, \tag{1b}$$

where θ and φ are the elevation and azimuth angles of the beam pointing, respectively, γ is the rotation angle of the radiation layer, d is the period of the transverse stub, ϵ_g is the effective dielectric constant, and λ is the wavelength in free space. (1a) and (1b) show that the beam pointing angles change with λ and γ.

The frequency scanning of the traditional VICTS antenna is caused by a 2π phase difference between the elements in the x- and y-directions. Therefore, to eliminate beam walk, every element should be fed separately. However, if every element is fed separately, the feeding network will be so complicated that it will be difficult to construct. Therefore, to alleviate beam squint, the whole array should be divided into subarrays of the appropriate size (Figure 2(b)), and the phase difference between each subarray should be compensated by the true time delay. The true time delay can be achieved based on the length difference of the waveguide between each subarray. The phase difference between each subarray will be discussed in terms of the x-direction and y-direction phase differences.

2.1. x-Direction Phase Difference. To simplify the design, the subarray in the x-direction can be corporate fed and the phase difference α_x between each subarray is

$$\alpha_x = k_0 u q \frac{d}{\cos(\gamma)}, \tag{2}$$

where q is an integer. Substituting (1a) and (1b) into (2), α_x can be simplified to $2q\pi$. This illustrates that the phase difference in the x-direction between each slot should be compensated by $2q\pi$. q changes with the rotation angle, and thus, it should be chosen carefully to achieve good performances at any rotation angle. The subarray dimensions in the x-direction should be the same, and the array arrangement should be optimized to achieve an acceptable compromise between the complexity of the feeding network and the aperture efficiency.

2.2. y-Direction Phase Difference. The y-direction phase difference is discussed in terms of subarrays on the same side of the rotation centre and those on opposite sides of the rotation centre. The phase difference of two VICTS subarrays on the same side of the rotation centre in the y-direction is shown in Figure 3. The phase difference between the outputs of the feeding networks of the two subarrays includes the phase difference determined by the free space path length differences and the phase difference caused by the waveguide path length differences, expressed as follows:

$$\alpha_y = k_0 v (L1 - L2 - W1 + W2) + k_e (W1 - W2), \tag{3}$$

where $k_0 = 2\pi/\lambda$ is the free-space wave number at frequency f_0, $k_e = k_0\sqrt{\epsilon_g}$ is the equivalent propagation constant in the waveguide, $W1$ ($W2$) is the distance between the output of the feeding network and the first slot centre of the 1st (2nd) subarray, and $L1$ ($L2$) is the distance between feeding position of the 1st (2nd) subarray and the rotation centre of the

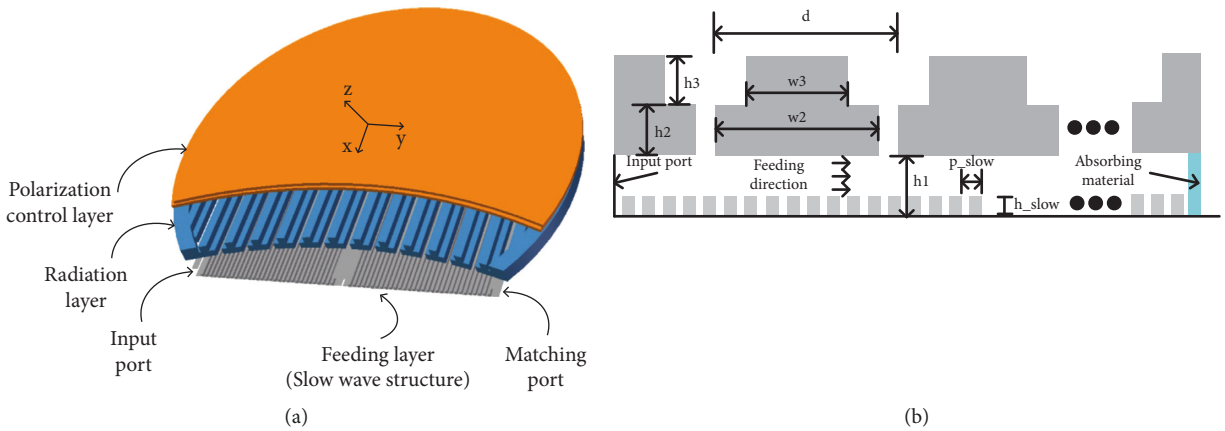

FIGURE 1: Diagrams of variable inclination continuous transverse stub (VICTS) antenna: (a) three-dimensional perspective and (b) side view.

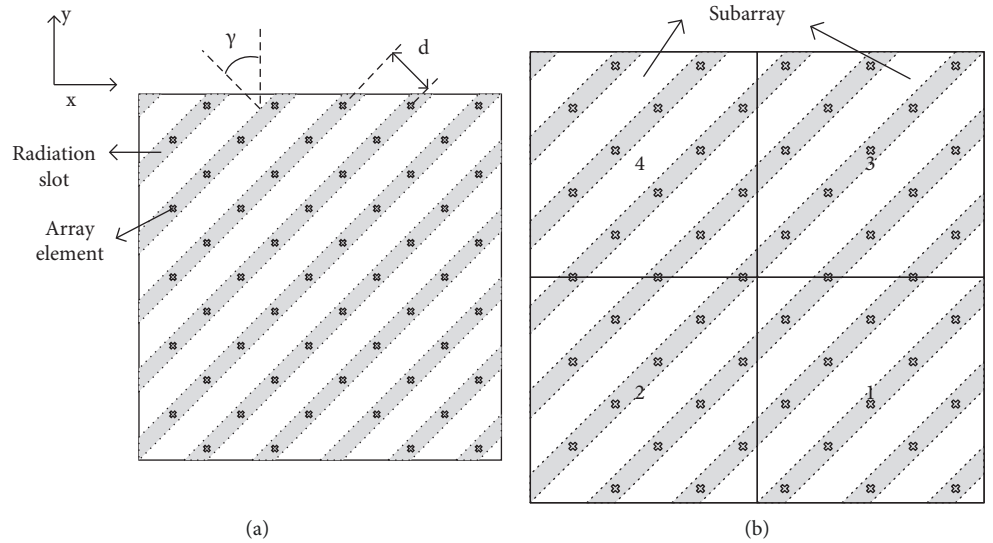

FIGURE 2: Rectangular array equivalent of (a) traditional and (b) proposed VICTS antennas.

radiation layer. It should be noted that (3) can be applied to both backward and forward radiation situations.

Figure 4 shows the waveguide path length differences when the rotation angle of the radiation layer is γ. $W1$ and $W2$ can be written as

$$W1 = L1 - \frac{L1 - d1 - l_{slot}/2 - m * d}{\cos(\gamma)}, \tag{4a}$$

$$W2 = L2 - \frac{L2 - d2 - l_{slot}/2 - n * d}{\cos(\gamma)}, \tag{4b}$$

where l_{slot} is the length of the slot, d is the period of the transverse stub, and m and n are integers. When the nearest radiation slot is the first slot, m and n are zero. The waveguide path length differences are then

$$W1 - W2 = L1 - L2 - \frac{L1 - L2 - d1 + d2 - m \times d + n \times d}{\cos(\gamma)}. \tag{5}$$

With equations (1a), (1b), and (5), equation (3) reduces to

$$\begin{aligned} \alpha_y &= -k_0 \frac{\lambda_0}{d} (L1 - L2 - d1 + d2 + m \times d - n \times d) \\ &\quad + k_0 \sqrt{\varepsilon} (L1 - L2) \\ &= -2\pi * \left(\frac{L1 - L2 - d1 + d2}{d} - m + n \right) \\ &\quad + k_0 \sqrt{\varepsilon} (L1 - L2), \end{aligned} \tag{6}$$

which shows that the phase difference is not related to the rotation angle.

The second scenario is when the two VICTS subarrays are on opposite sides of the rotation centre, as shown in Figure 5. The phase difference α_y is the same as that in the first situation and can be written as

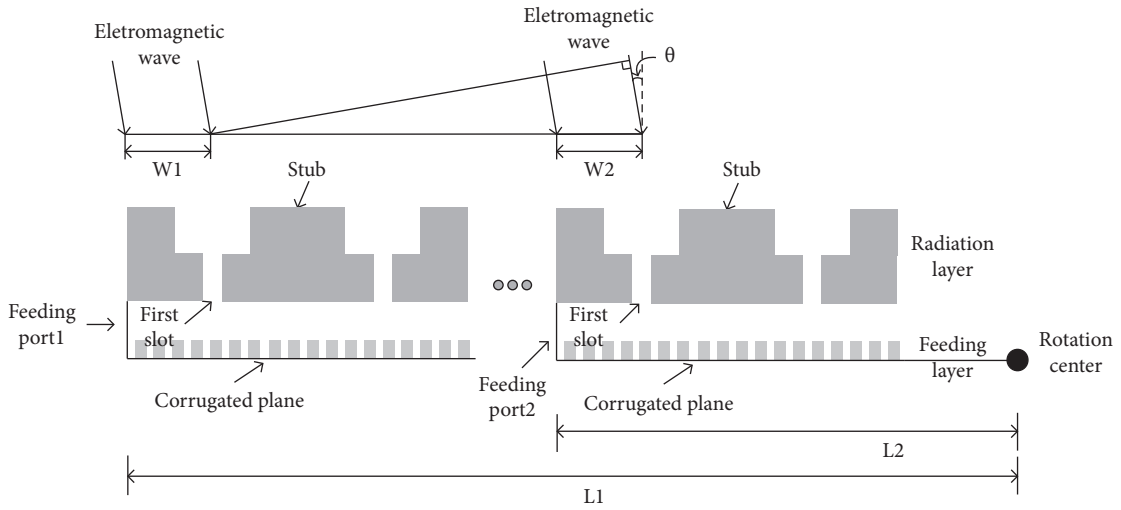

Figure 3: Phase difference between two VICTS subarrays on the same side of the rotation centre in the y-direction.

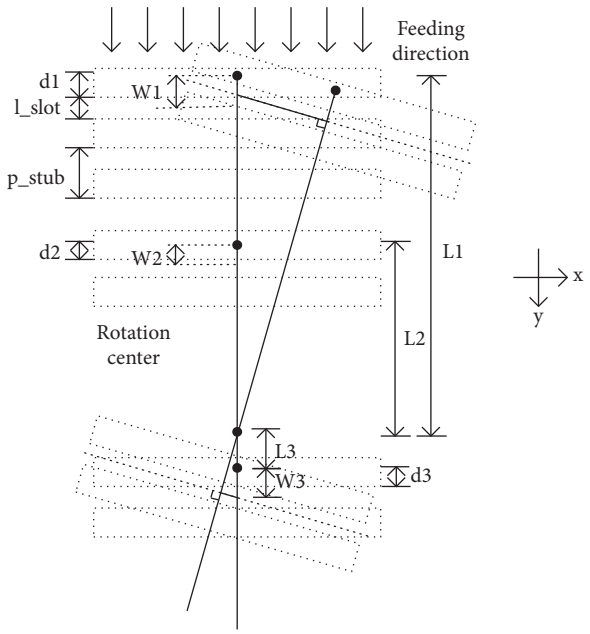

Figure 4: Waveguide path length difference of two VICTS subarrays in the y-direction.

$$\alpha_y = k_0 v(L1 + L1 - \mathrm{W1} + \mathrm{W3}) + k_e(\mathrm{W1} - \mathrm{W3}). \quad (7)$$

The waveguide path length and path length differences are shown in Figure 4 are

$$W1 = L1 - \frac{L1 - d1 - l_{slot}/2 - m * d}{\cos(\gamma)}, \quad (8a)$$

$$W3 = \frac{L3 + d3 + l_{slot}/2 - p * d}{\cos(\gamma)} - L3, \quad (8b)$$

$$W1 - W3 = L1 + L3 - \frac{L1 + L3 - d1 + d3 - m * d + p * d}{\cos(\gamma)}, \quad (9)$$

where p is an integer. Therefore, the phase difference can be simplified as

$$\alpha_y = -\frac{2\pi}{d}(L1 + L3 - d1 + d3 - m * d + p * d) + k_0\sqrt{\varepsilon}(L1 + L3). \quad (10)$$

It should again be noted that the phase differences between the two situations are equal.

To allow the phase difference to be easily determined, $L1 - L2$ or $L1 + L3$ in (6) and (10), respectively, should be multiples of d and $d1$, $d2$, and $d3$ should be equal, which is consistent with the results of Hao et al. [6]. When $d1$, $d2$, and $d3$ are equal, the phase difference can be determined by

$$\alpha_y = v_0\frac{(L1 - L2)}{c}, \quad (11a)$$

or

$$\alpha_y = v_0\frac{(L1 + L3)}{c}, \quad (11b)$$

where v_0 is the beam pointing angle when the rotation angle is 0 at the centre frequency, ω_0 is the centre angular frequency, and c is the speed of light in free space. The time delay T is computed by

$$T = \alpha/(2\pi f_0), \quad (12)$$

where f_0 is the centre frequency of the bandwidth.

The phase difference is changed by m, n, and p, which means the phase difference varies with the rotation angle. Therefore, the beam squint will deteriorate as the rotation angle changes. To maintain the performance at any rotation angle, the time-delay compensation in the y-direction can be determined by setting $W1 - W2 = 0$.

Thus,

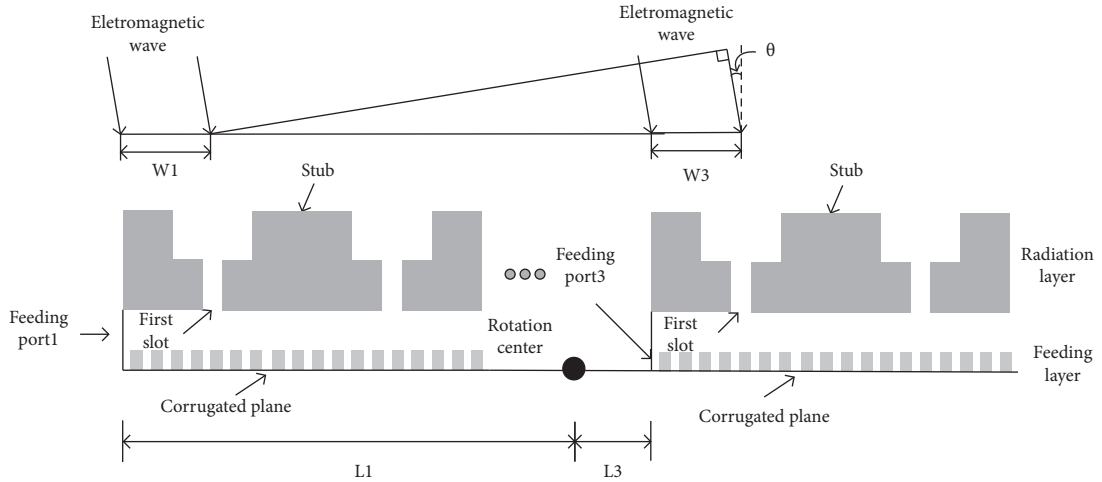

Figure 5: Wavelength difference of two VICTS subarrays on opposite sides of the rotation centre in the y-direction.

$$\cos(\gamma) = \frac{L1 - L2 + d1 - d2 - m \times d + n \times d}{L1 - L2}$$
$$\gamma = \arccos\left(\frac{L1 - L2 - m \times d + n \times d}{L1 - L2}\right). \quad (13)$$

3. Simulation Results and Discussion

To demonstrate the presented methodology, a VICTS antenna composed of 2×2 subarrays was designed and simulated using CST Microwave Studio software. Each subarray was fed by a waveguide port, and the port mode was transverse electromagnetic (TEM) mode, which is shown in Figure 6. The port mode was guaranteed by designing feeding networks and parallel plate waveguide height. The feeding network design is not the main focus of this paper. The height of the parallel plate waveguide was less than half the wavelength, which means the TM_n (TM: transverse magnetic) and TE_n (TE: transverse electric) modes were suppressed in the structure. To ensure that there was no influence between each unit, an absorbing material was placed at the end of each subarray (Figure 1(b)). The true-time delay was implemented by introducing a time shift between each port. The excitation type was simultaneous.

The parameters were $h1 = 10$ mm, $h2 = 5$ mm, $h3 = 6$ mm, $d = 20$ mm, $w2 = 17$ mm, $w3 = 6$ mm, $p\_\text{slow} = 2$ mm, and $h\_\text{slow} = 2$ mm. S_{11} of each subarray at rotation angles of 0°, 15°, 33.56°, and 42° was below −15 dB from 11 to 13 GHz, which is shown in Figure 7. The subarray spacing in the y-direction ($L1 - L2$) was set to 6 d, and γ was calculated from equation (13) to be 33.56° by setting $m = 1$ and $n = 0$. The time compensation in the y-direction was computed at the rotation angles of 0° and 33.56° using (6), (10), and (12), and the time compensation in the x-direction was stepped at 2π intervals. We introduced the gain loss to analyse the performance of the antenna. The gain loss [10] is the gain difference between the centre frequency and other frequencies in the beam direction of the centre frequency.

The gain losses with different rotation angles and amounts of time compensation are shown in Table 1. With the increase in the compensation in the x-direction, the gain loss at the rotation angle of 0° was increased, while the gain loss at the rotation angle of 33.56° was reduced. For the y-direction, the compensation at the rotation angle of 33.56° had a lower beam walk than the compensation at the rotation angle of 0°. The performance at high frequencies was better than that at low frequencies, because the gain at high frequencies was higher.

The time offset should be set to make the beam walk at any rotation angle stable. A 4π offset in the x-direction and y-direction offset at the rotation angle of 33.56 using(6), (10), and (12) was chosen for this time offset, which was suitable for a middle rotation angle while maintaining the same performance at other rotation angles, and the gain losses were less than 0.75 dB. The patterns of the antenna are shown in Figure 8. The sidelobe level was lower than −10 dB. Moreover, an unequal power divider could be used in the future to reduce the sidelobe level.

The gain at 12 GHz and gain losses at 11.75 and 12.25 GHz and those of the traditional VICTS antenna are listed in Table 2 at rotation angles of 0°, 15°, 33.56°, and 45°. The gain of the proposed antenna was about 2 dB lower than that of the traditional VICTS antenna because the feeding network reduced the aperture efficiency. However, the gain can be increased by introducing more elements at the edge, which cannot be achieved by the traditional VICTS antenna. Compared to the traditional antenna, the gain loss was reduced by at least 52% and the 3/4-dB gain loss bandwidth increased from 2.5% to 4.2%.

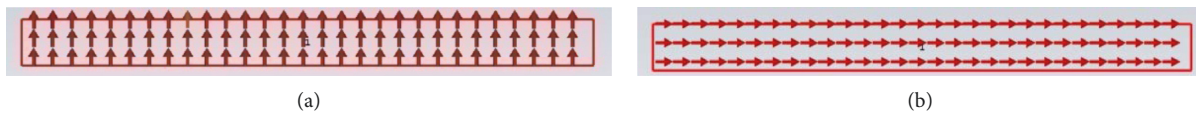

(a) (b)

Figure 6: Port mode: (a) Electric field. (b) Magnetic field.

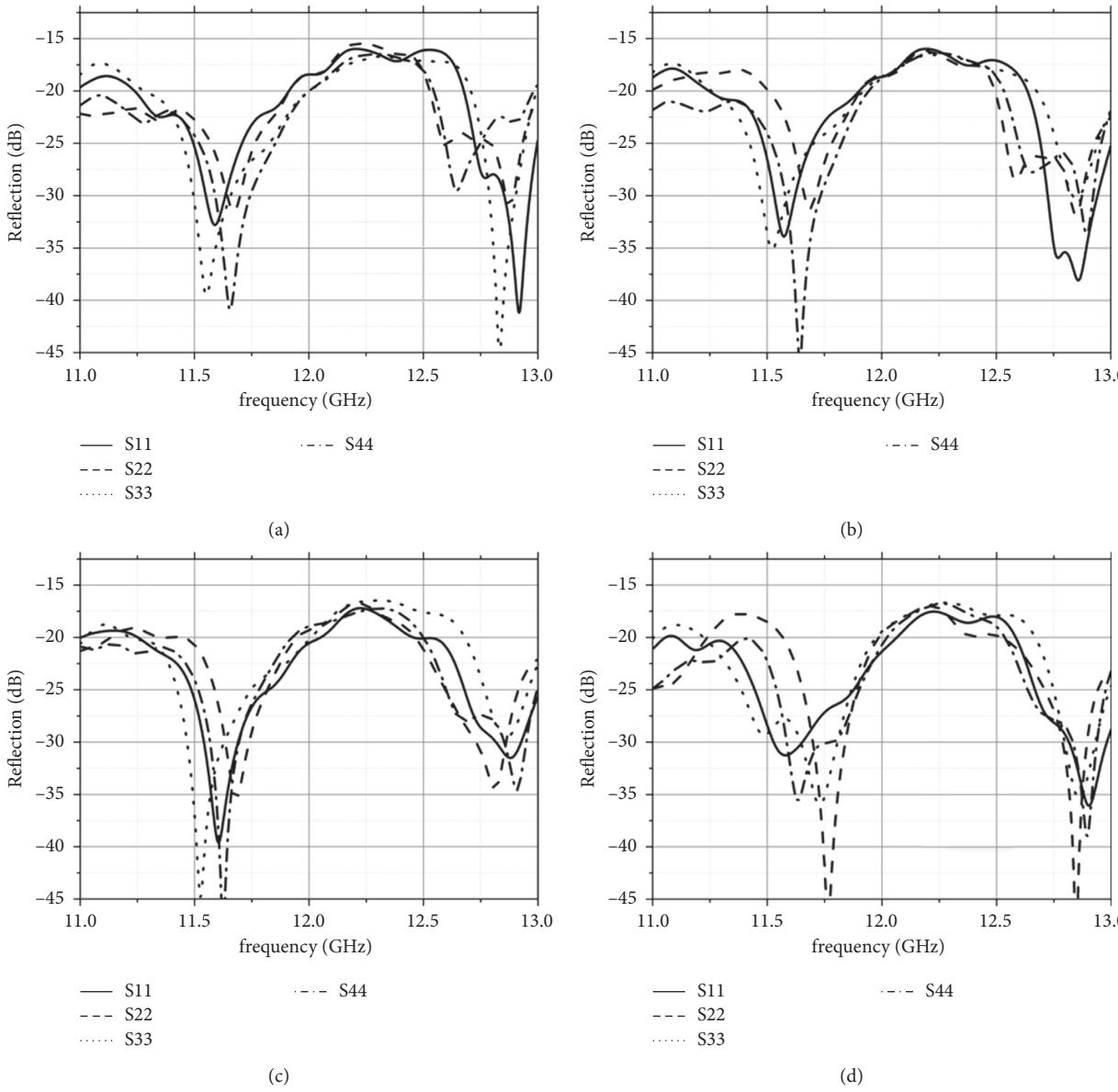

Figure 7: S parameters of each subarray. Rotation angles of (a) 0°, (b) 15°, (c) 33.56°, and (d) 42°.

Table 1: Gain losses for different rotation angles and time compensations.

Gain loss	0		15		33.56		42	
(X, Y)	11.75	12.25	11.75	12.25	11.75	12.25	11.75	12.25
(0, 33.56)	0.16	0.71	0.25	0.6	0.62	0.13	0.91	0.48
$(2\pi, 33.56)$	0.17	0.73	0.21	0.55	0.49	0.05	0.76	0.34
$(4\pi, 33.56)$	0.23	0.75	0.21	0.54	0.39	0	0.63	0.24
(0, 0)	0.31	0.57	0.41	0.41	0.89	−0.01	1.07	0.37
$(2\pi, 0)$	0.33	0.59	0.36	0.37	0.75	−0.09	0.92	0.23
$(4\pi, 0)$	0.38	0.65	0.36	0.37	0.66	−0.14	0.81	0.13

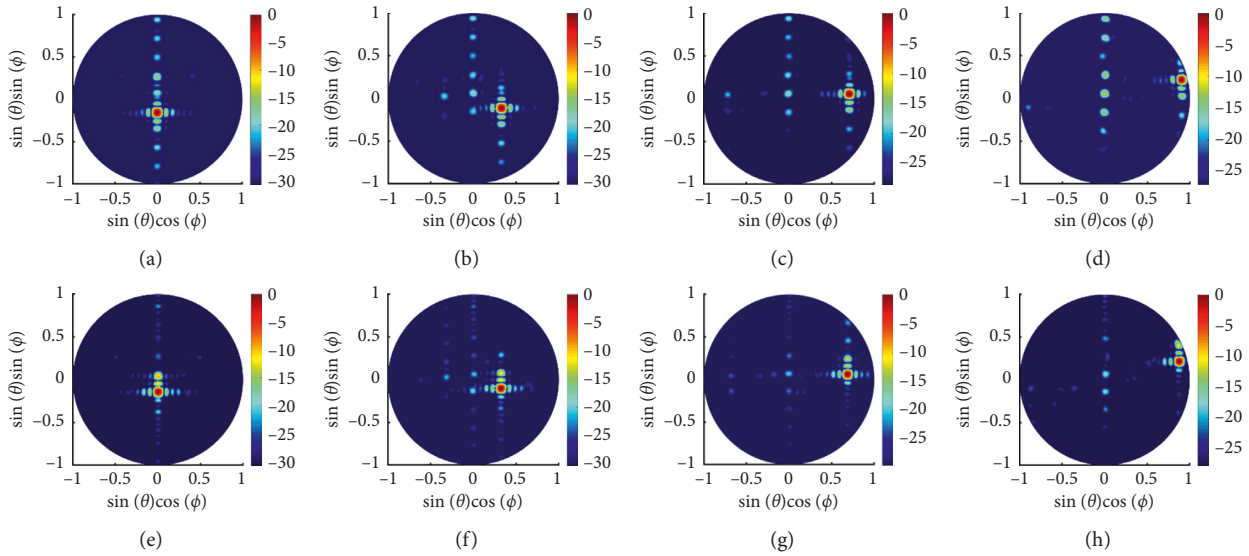

Figure 8: Simulated patterns, where the colour represents the dB level: (a–d) 11.75 GHz and (e–h) 12.25 GHz. Rotation angles of (a) 0°, (b) 15°, (c) 33.56°, (d) 42°, (e) 0°, (f) 15°, (g) 33.56°, and (h) 42°.

Table 2: Gain at 12 GHz and gain loss at 11.75 and 12.25 GHz compared with the traditional VICTS antenna.

Rotation angle	Proposed VICTS		Traditional VICTS	
	Gain	Gain loss (11.75, 12.25)	Gain	Gain loss (11.75,12.25)
0	24.3	(0.23, 0.75)	25.4	(0.94, 0.88)
15	24.06	(0.21, 0.54)	26.19 s	(1.26, 1.05)
33.56	23.03	(0.39, 0)	25.22	(0.76, 1.1)
42	22.28	(0.63, 0.24)	24.23	(1.43, 0.71)

4. Conclusions

A theoretical analysis and design methodology of the instantaneous bandwidth enhancement of the VICTS antenna were presented. The design methodology was verified by simulations. Compared to the traditional VICTS antenna, the gain loss of the proposed antenna was reduced by at least 52% and the 3/4-dB gain loss bandwidth reached 4.2%. The S_{11} was below −15 dB over a frequency range of 11–13 GHz. The sidelobe of the array was lower than −10 dB. The antenna radius was 0.34 m, and the aperture efficiency was 14.8%. The proposed antenna is a suitable candidate as a gateway station antenna for low earth orbit satellite communication.

Data Availability

The data used to support the findings of this study are available from the corresponding author upon request.

Conflicts of Interest

The authors declare that there are no conflicts of interest regarding the publication of this paper.

References

[1] A. H. Aljuhani, T. Kanar, S. Zihir, and G. M. Rebeiz, "A 256-element ku-band polarization agile SATCOM receive phased array with wide-angle scanning and high polarization purity," *IEEE Transactions on Microwave Theory and Techniques*, vol. 69, no. 5, pp. 2609–2628, 2021.

[2] Ke Chen, Ze-H. Yan, B. Wen, and T.-L. Zhang, "High efficiency dual polarization flat panel antenna for mobile satellite communication," in *Proceedings of the 2013 International Workshop on Microwave and Millimeter Wave Circuits and System Technology*, pp. 58–61, IEEE, Chengdu, 24-25 October 2013.

[3] M. Alibakhshikenari, B. Virdee, P. Shukla et al., "Antenna mutual coupling suppression over wideband using embedded periphery slot for antenna arrays," *Electronics*, vol. 7, p. 198, 2018.

[4] Y. Shang, W. Zhou, and C. Liao, "Metasurface-based cylindrical lenses and their antenna gain enhancement," *International Journal of Antennas and Propagation*, vol. 2020, pp. 1–14, 2020.

[5] B. G. Porter, "Closed form expression for antenna patterns of the variable inclination continuous transverse stub," in *Proceedings of the 2010 IEEE International Symposium on Phased Array Systems and Technology*, pp. 164–169, Waltham, MA, USA, 12-15 October 2010.

[6] J. Gao, X. Lei, G.-H. Chen, Y. Zhang, and J.-M. Wu, "Design of the variable inclination continuous transverse stub antenna based on rectangular grating slow-wave structure," *International Journal of Antennas and Propagation*, vol. 1, p. 7, 2018 5793535.

[7] R. S. Hao, Y. J. Cheng, and Y. F. Wu, "Shared-aperture variable inclination continuous transverse stub antenna working at K- and ka-bands for mobile satellite communication," *IEEE Transactions on Antennas and Propagation*, vol. 68, no. 9, pp. 6656–6666, 2020.

[8] K. Tekkouk, J. Hirokawa, R. Sauleau, and M. Ando, "Wideband and large coverage continuous beam steering antenna in the 60-GHz band," *IEEE Transactions on Antennas and Propagation*, vol. 65, no. 9, pp. 4418–4426, 2017.

[9] W. Yuan, J. F. Chen, C. Zhang et al., "Glide-symmetric lens antenna in gap waveguide technology," *IEEE Transactions on Antennas and Propagation*, vol. 68, no. 4, pp. 2612–2620, 2019.

[10] R. Mailloux, *Phased Array Antenna Handbook*, Artech, Third Edition, 2017.

[11] M. Jung and B.-W. Min, "A compact 3–30-GHz 68.5-ps CMOS true-time delay for wideband phased array systems," *IEEE Transactions on Microwave Theory and Techniques*, vol. 68, no. 12, pp. 5371–5380, 2020.

[12] "Optimized true-time delay beam-stabilization techniques for instantaneous bandwith enhancement," United State Patent No.2018069321A1, 2014.